Feasibility of Dual-frequency Conductivity Imaging using MREIT and MREPT

Atul S. Minhas, Young Tae Kim, Hyung Joong Kim, Eung Je Woo
Impedance Imaging Research Center and Department of Biomedical Engineering
Kyung Hee University
Gyeonggi-do, Korea

Min-oh Kim, Dong-Hyun Kim
Department of Electrical and Electronic Engineering
Yonsei University
Seoul, Korea

Jin Keun Seo
Department of Computational Science & Engineering
Yonsei University
Seoul, Korea

***Abstract*—Magnetic resonance electrical impedance tomography (MREIT) and magnetic resonance electrical property tomography (MREPT) are new medical imaging modalities capable of visualizing distributions of electrical properties inside an electrically conducting object such as the human body. MREIT provides conductivity images at frequencies below a few kHz by processing MR phase images subject to externally injected currents, while MREPT provides both conductivity and permittivity images at the Larmor frequency (128 MHz at 3 T) by processing B1 maps. In this paper, we present experimental results of both MREIT and MREPT and highlight their distinct features in probing and visualizing the same object.**

Keywords-MREIT, MREPT, conductivity, permittivity

I. INTRODUCTION

Magnetic resonance electrical impedance tomography (MREIT) and magnetic resonance electrical property tomography (MREPT) are new imaging modalities capable of visualizing electrical properties of the human body using an MRI scanner. MREIT provides conductivity images at frequencies below a few kHz whereas MREPT produces both conductivity and permittivity images at the Larmor frequency which is about 128 MHz at 3 T, for example.

In MREIT, we inject low-frequency currents to induce extra magnetic fields, whose z-components are measured from MR phase images using an MRI scanner with its main field in the z-direction. MREIT produces low-frequency conductivity images using the acquired induced magnetic flux density maps based on their relation to the conductivity distribution [1,2]. Without injecting current, MREPT relies on acquired B1 maps, which are influenced by both the conductivity and permittivity distributions at the Larmor frequency [3].

Biological tissues show frequency-dependent conductivity and permittivity spectra and their values at different frequencies may provide valuable diagnostic information. MREIT and MREPT are, therefore, supplementary to each other and can provide new information when combined together.

In this study, we address this issue and present distinct differences between MREIT and MREPT in reconstructed conductivity images from phantom experiments. Considering pros and cons of these methods and also the fact that the conductivity of a biological tissue changes with frequency, we will propose a dual-frequency MR-based conductivity imaging method combining MREIT and MREPT together.

II. METHODS

A. MREIT Phantom Experiments

We constructed a cylindrical phantom with 13 cm diameter and 16 cm height (Fig. 1). We filled it with a saline of 0.12 S/m conductivity (0.15 g/l NaCl and 2 g/l CuSO4). Inside the phantom, we placed two cylindrical agar gel objects with 2.79 S/m (right side in Fig. 1a) and 1.14 S/m (left side in Fig. 1a). All the conductivity values were measured using the four-electrode method with an impedance analyzer. We attached four carbon-hydrogel electrodes (HUREV Co. Ltd., Korea) around the phantom and sequentially injected currents I_1 and I_2 at two different directions through two pairs of opposing electrodes.

We placed each phantom inside the bore of our 3 T MRI scanner (Magnum 3, Medinus Co. Ltd., Korea). Using a custom-designed MREIT current source [4], we injected 3 mA currents as the first currents I_1 between the horizontal pair of electrodes. After acquiring the first data set with I_1 in 8 axial slices, the second injection currents I_2 with the same amplitude and width were injected through the vertical pair of electrodes. Imaging parameters were as follows: TR/TE = 1000/20 ms, number of echoes = 6, FOV = 180×180 mm^2, matrix size = 128×128, slice thickness = 4 mm, number of slices = 8, NEX = 12 and total imaging time = 100 min.

B. MREPT Phantom Experiment

Fig. 2(a) shows an MR magnitude image of a phantom including three cylindrical anomalies with different conductivity values. The background was a mixture of 3 L distilled water and 75 g agar powder. For the three anomalies of agar gels, we used 1.5, 3, and 4.5% NaCl solutions with 2.5% agar powder to produce three different conductivity values. We wrapped each agar gel object with a thin plastic film to prevent any ion diffusion from altering its conductivity. All three agar gel objects and the background had 0.2% $CuSO_4$ to reduce their T1 values.

We employed a B1 mapping scheme based on the Double Angle Method (DAM) [5,6]. We acquired a set of spin echo images using 60° to 180° flip angles and 120° to 180° flip angles. We obtained the magnitude of H^+ by computing $\cos^{-1}(M_2/2M_1)$ where M_1 and M_2 correspond to the image magnitudes acquired from the 60° to 180° and 120° to 180° flip angles acquisitions, respectively. The phase of H^+ was obtained from the DAM acquisition data by retrieving the one-half value of the phase [7]. Imaging parameters were as follows: main field strength = 3 T, TR/TE = 600/20 ms, FOV = 180×180 mm^2, resolution = 1.4×1.4 mm^2, slice thickness = 4 mm, 8 slices, and quadrature transmit/receive coil. To deal with noise, we used a Gaussian filter of a varying size.

C. Dual-frequency Imaging of MREIT and MREPT

We conducted both MREIT and MREPT imaging experiments using two specially constructed conductivity phantoms to distinguish their features. We prepared two kinds of cylindrical agar gel objects with 1.14 and 2.79 S/m conductivity values. We wrapped those agar gel objects with thin plastic films and placed them inside the first phantom. In the second phantom with the same size, we placed the agar gel objects without using the thin plastic wrap. We filled the backgrounds of both phantoms with a saline of 0.12 S/m conductivity value. We expected that the wrapped agar gel objects should appear as insulators in an MREIT image since injected low-frequency current cannot penetrate the plastic films. However, the same wrapped agar gel objects should show their conductivity values in an MREPT image since the thin films are transparent to the electromagnetic wave at the Larmor frequency of 128 MHz. Both of the unwrapped agar gel objects should show their conductivity values in both MREIT and MREPT images.

For the MREIT experiment, we used a spin echo based B_z field mapping sequence for data collections and the harmonic B_z algorithm for scaled conductivity image reconstructions [1,8-11]. The injected current amplitude was 3 mA with 85 ms pulse width. The MREPT experiment was performed separately using the method described above. Both experiments were conducted on a 3 T MRI scanner.

III. Results

A. MREIT Images at about 100 Hz

Fig. 1 shows the results of typical MREIT experiment using the agar gel phantom. Fig. 1(a) is its MR magnitude image and (b) and (c) are magnetic flux density images subject to horizontal and vertical current injections, respectively, and (d) is a reconstructed conductivity image. Conductivity images show clear contrast between two different agar objects.

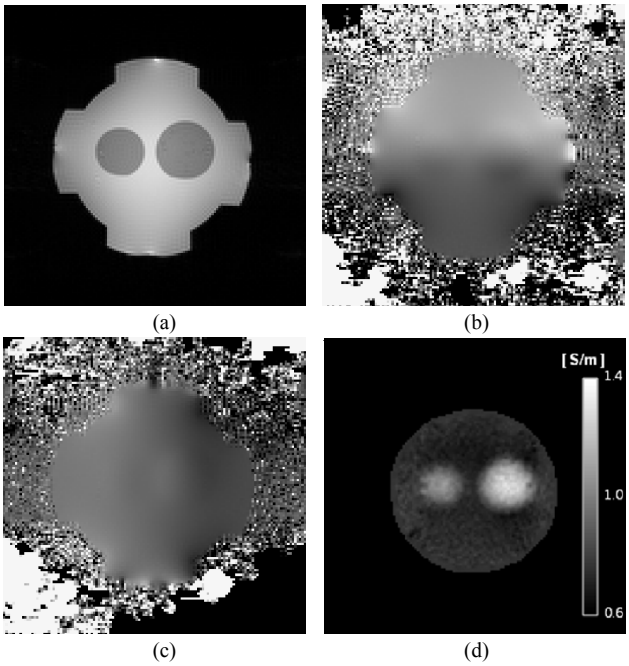

Figure 1. MREIT imaging experiment using a phantom including two different agar gel objects. (a) MR magnitude image, (b) and (c) magnetic flux density images subject to horizontal and vertical current injections, respectively, and (d) reconstructed conductivity image.

B. MREPT Images at 128 MHz

Fig. 2 shows the results of the MREPT experiment. In the MR magnitude image, the dark circular rings are the thin plastic cylindrical films which wrapped the three anomalies to maintain them as regions of constant conductivity values. From the acquired B1 phase and magnitude maps, we reconstructed the conductivity image, which recovered conductivity values inside the three homogeneous anomalies. Around the boundary of each anomaly where the assumption of the local homogeneity is not satisfied, we observed dark circular rings where conductivity values were not properly recovered.

C. MREIT and MREPT Dual-frequency Images

As shown in Fig. 3, the wrapped agar gel objects appeared as insulators in the low-frequency conductivity image from the MREIT experiment. On the other hand, the high-frequency conductivity image from the MREPT experiment showed their conductivity values without being affected by the thin insulating films.

Both MREIT and MREPT recovered conductivity contrasts of the unwrapped agar objects. For both wrapped and unwrapped agar objects, the reconstructed MREPT images show erroneous regions around the boundaries of the objects.

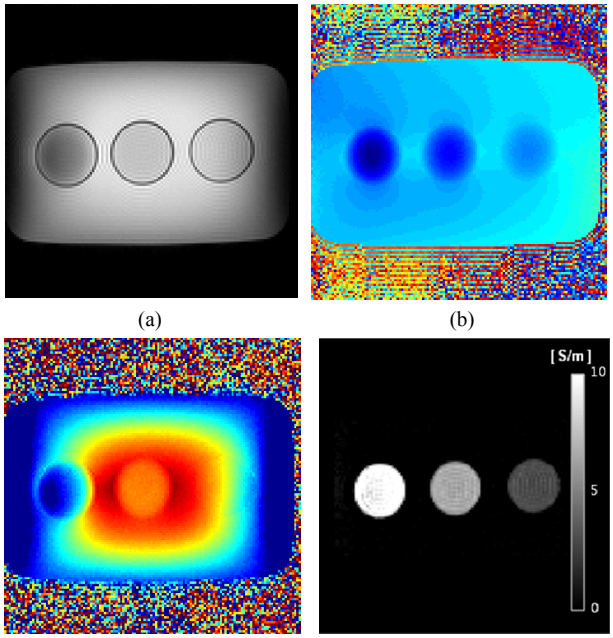

Figure 2. MREPT imaging experiment using a phantom including three different agar gel objects. (a) MR magnitude image, (b) B1 phase image, (c) B1 magnitude image, and (d) reconstructed conductivity image.

IV. Discussion and Conclusion

MREIT and MREPT images clearly show distinct properties of the two methods. MREIT provides conductivity images at a low frequency whereas MREPT produces conductivity images at the Larmor frequency of 128 MHz at 3 T. MREPT does not require any current injection whereas MREIT does.

As illustrated in Fig. 3, MREIT is advantageous in seeing an anomaly itself which is wrapped with a thin insulating membrane. If the membrane is porous, MREIT will be able to quantitatively visualize the membrane property as well. Though MREPT fails to see such membranes, it will be able to probe things inside an insulating membrane. Some biological tissues such as the muscle and white matter are anisotropic at low frequencies but they become isotropic at high frequencies above 10 MHz, for example [12,13]. MREIT is potentially capable of sensing the effects of tissue anisotropy whereas MREPT being at its early stage needs further development to detect anisotropic conductivity. Considering these pros and cons and also the fact that conductivity of a biological tissue changes with frequency, we suggest a dual-frequency conductivity imaging incorporating both MREIT and MREPT.

In MREIT, we reconstruct low-frequency conductivity images from induced magnetic field maps subject to externally injected currents. Positive and negative currents with the same amplitude are injected and the magnetic field maps are obtained from the phase difference of the two acquisitions. For MREPT, both magnitude and phase information of B1 maps are used to produce high frequency conductivity images. Conductivity is mainly influenced by the phase while permittivity is mostly dominated by the magnitude of a B1 map. We note that the same DAM method employed for B1 mapping can also be used to acquire MREIT data. This is considering the fact that we acquire the B1 mapping data while injecting current of two opposite polarities for MREIT. To obtain the B1 map from such data, we may cancel the current injection induced phase by adding the two phases due to opposite current injection polarities. We, therefore, suggest performing MREIT and MREPT simultaneously by properly manipulating acquired phase information.

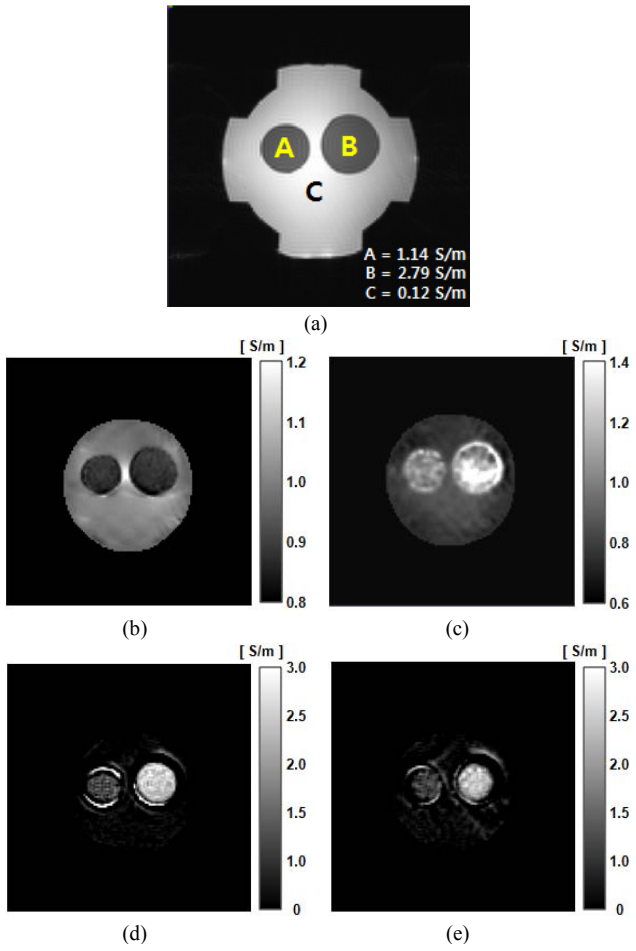

Figure 3. Dual-frequency conductivity imaging experiment using MREIT and MREPT. (a) MR magnitude image of a phantom including two different agar gel objects. (b) and (c) reconstructed low-frequency conductivity images from MREIT. (d) and (e) reconstructed high-frequency conductivity images from MREPT. In (b) and (d), both agarose anomalies were wrapped by thin insulating films whereas they were not wrapped in (c) and (e).

Acknowledgment

This work was supported by the National Research Foundation of Korea (NRF) grant funded by the Korea government (MEST) (No. 20100018275).

References

[1] E. J. Woo, J. K. Seo, "Magnetic resonance electrical impedance tomography (MREIT) for high-resolution conductivity imaging", Physiol. Meas., vol. 29, pp. R1-26, 2008

[2] J. K. Seo, E. J. Woo, "Magnetic resonance electrical impedance tomography (MREIT)", SIAM Review, 2011.

[3] U. Katscher, T. Voigt, C. Findeklee, P. Vernickel, K. Nehrke, and O. Dossel, "Determination of electrical conductivity and local SAR via B1 mapping", IEEE Trans. Med. Imag., vol. 28, pp. 1365-1374, 2009.

[4] T. I. Oh, Y. Cho, Y. K. Hwang, S. H. Oh, E. J. Woo, S. Y. Lee, "Improved current source design to measure induced magnetic flux density distributions in MREIT", J Biomed. Eng. Res., vol. 27, pp. 30-37, 2006.

[5] R. Stollberger, P. Wach, "Imaging of the active B1 field in vivo", Magn. Reson. Med., vol. 35, pp. 246-251, 1996.

[6] P. F. van de Moortele, C. Akgun, G. Adriany, S. Moeller, J. Ritter, C.M. Collins, M. B. Smith, J. T. Vaughan, and K. Ugurbil, "B(1) destructive interferences and spatial phase patterns at 7 T with a head transceiver array coil", Magn. Reson. Med., vol. 54, pp. 1503-1518, 2005.

[7] H. Wen, "Noninvasive quantitative mapping of conductivity and dielectric distributions using RF wave propagation effects in high-field MRI", Proc. SPIE, vol. 5030, pp. 471-477, 2003.

[8] S. H. Oh, B. I. Lee, E. J. Woo, S. Y. Lee, M. H. Cho, O. Kwon, and J. K. Seo, "Conductivity and current density image reconstruction using harmonic B_z algorithm in magnetic resonance electrical impedance tomography", Phys. Med. Biol., vol. 48, pp. 3101-3016,2003.

[9] J. K. Seo, J. R. Yoon, E. J. Woo, and O. Kwon, "Reconstruction of conductivity and current density images using only one component of magnetic field measurements", IEEE Trans. Biomed. Eng., vol. 50, pp. 1121-1124, 2003.

[10] K. Jeon, H. J. Kim, C. O. Lee, E. J. Woo, J. K. Seo, "CoReHA: conductivity reconstructor using harmonic algorithms for magnetic resonance electrical impedance tomography (MREIT)", J. Biomed. Eng. Res., vol. 30, pp. 279-287, 2009.

[11] J. K. Seo, S. W. Kim, S. Kim, J. J. Liu, E. J. Woo, K. Jeon, C. O. Lee, "Local harmonic Bz algorithm with domain decomposition in MREIT: computer simulation study", IEEE Trans. Med. Imag., vol. 27, pp. 1754-1761, 2008.

[12] C. Gabriel, S. Gabriel, E. Corthout, "The dielectric properties of biological tissues: I. Literature survey", Phys. Med. Biol., vol. 41, pp. 2231-2249, 1996.

[13] S. Gabriel, R. W. Lau, C. Gabriel, "The dielectric properties of biological tissues: II. Measurements in the frequency range 10 Hz to 20 GHz", Phys. Med. Biol., vol. 41, pp. 2251-2269, 1996.